Science in China Series E: Technological Sciences

© 2009 SCIENCE IN CHINA PRESS
Springer

www.scichina.com
tech.scichina.com
www.springerlink.com

Effect of atomization gas pressure variation on gas flow field in supersonic gas atomization

ZHAO XinMing[1], XU Jun[1,2 †], ZHU XueXin[1] & ZHANG ShaoMing[1]

[1] National Engineering and Technological Research Center for Non-Ferrous Metals Composites, General Research Institute for Non-Ferrous Metals, Beijing 100088, China;
[2] Beijing COMPO Solder Co. Ltd., Beijing 100088, China

In this paper, a computational fluid flow model was adopted to investigate the effect of varying atomization gas pressure (P_0) on the gas flow field in supersonic gas atomization. The influence of P_0 on static pressure and velocity magnitude of the central axis of the flow field was also examined. The numerical results indicate that the maximum gas velocity within the gas field increases with increasing P_0. The aspiration pressure (ΔP) is found to decrease as P_0 increases at a lower atomi- zation gas pressure. However, at a higher atomization gas pressure increasing P_0 causes the opposite: the higher atomization gas pressure, the higher aspiration pressure. The alternation of ΔP is caused by the variations of stagnation point pressure and location of Mach disk, while hardly by the location of stagnation point. A radical pressure gradient is formed along the tip of the delivery tube and increases as P_0 increases.

gas atomization, atomization gas pressure, gas flow field, numerical simulation

1 Introduction

Over the past decades, gas atomization technique has been paid considerable attention as a flexibility process for the production of a wide range of ultrafine spherical metal powders, which have very attractive properties as a result of high cooling rate (10^4-10^6℃/s) and deep under-cooling powders experience[1]. In the gas atomization process, atomization gas pressure P_0 plays an important role in determining the particle size and surface morphology. Several studies have been carried out on the effect of P_0 on the particle characteristics[2−6]. Yu et al.[2] showed that at P_0=0.7 MPa, the Sn63Pb solder alloy powders were more uniform, without satellite particles, and with a smaller median particle size, and that when P_0 was above or below 0.7 MPa, the powder of poor performance was obtained. However, Aksoy et al.[3−6] found that the median particle size decreased as P_0 increased. In despite of the importance of atomization gas pressure, the physics of the effect of P_0 on the powder characteristics was not understood well. Recently, efforts to understand it have been made in several research groups[7−13]. Ting et al.[7] investigated the "open-wake" and "closed-wake" phenomena as the atomization gas pressure varied in HPGA nozzle, and a pulsatile atomization model was presented. Mi et al.[8,9] simulated the effects of atomization gas pressure and melt tip geometry on the HPGA gas flow field by using computational fluid dynamics software PHOENICS. Jeyakumar et al.[10] presented a model of gas flow inside and outside of the convergent nozzle using software Fluent. Tong et al.[11] investigated the dynamics interactions between melt and atomization gas near the nozzle at the start of atomization using a front-tracking formulation. Zeoli et al.[12] simulated the process of metal droplet break-up, cooling and solidi

Received November 16, 2008; accepted March 2, 2009
doi: 10.1007/s11431-009-0158-5
†Corresponding author (email: xujun@grinm.com)
Supported by the National Engineering Technology Research Center Development Program (Grant No. NCSTE-2007-JKZX-054)

Citation: Zhao X M, Xu J, Zhu X X, et al. Effect of atomization gas pressure variation on the gas flow field in supersonic gas atomization. Sci China Ser E-Tech Sci, 2009, 52(10): 3046−3053, doi: 10.1007/s11431-009-0158-5

fication in an isentropic plug nozzle (IPN) during gas atomization. Allimant et al.[13] studied the influences of melt flow rate and the autoclave pressure on gas flow field for de Laval nozzle. However, few investigations have focused on the changes of gas flow field in close-coupled supersonic gas atomization nozzle (the nozzle has a Laval design) due to the alternation of P_0.

It has been reported that a good correlation exists between the gas-only flow condition and melt-gas flow condition[8]. In the present study, based on the close-coupled supersonic gas atomization nozzle configuration, a computational fluid flow model was used to investigate the effect of P_0 on gas flow field, and to explore the alteration of some atomization parameters. The knowledge gained from this model would be used to develop the rule and guidance for the design and the operation of high efficient atomization nozzle, and to understand the phenomenon occurred during gas atomization process.

2 Description of physical model

A supersonic gas atomization nozzle designed by ourselves was employed in this investigation. Figure 1 shows a schematic diagram of the atomization nozzle, where α is the jet included angle, β is the apex angle of metal delivery tube and h is the protrusion length of metal delivery tube. The nozzle has a common manifold with a single inlet connected to a high pressure gas container. The inlet pressure is monitored by a regulator and the atomization gas is nitrogen.

In order to establish the model of atomization gas flow, assumptions were made as follows.

1) The gas flow is in a steady state.

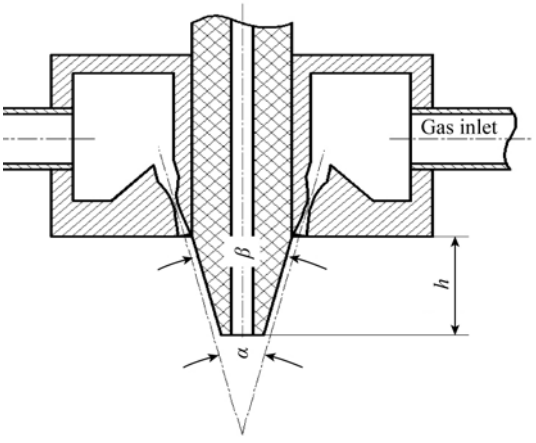

Figure 1 Schematic of the close-coupled supersonic atomization nozzle (CCSN).

2) The gas field as well as the nozzle manifold is axis-symmetric about the atomization nozzle centerline. In order to reduce the computational time, a two-dimensional (2D) axis-symmetric model is adopted.

3) The gas flow is isentropic compressible, and obeys the perfect gas law $P = \rho RT$.

4) The gas flow is turbulent fluid, and there are momentum and energy transfers between flow layers.

5) The effect of gravity is neglected.

3 Numerical model and computational methods

3.1 Governing equations

The continuity equation is

$$\frac{\partial}{\partial x_i}(\rho \boldsymbol{u}_i) = 0 . \tag{1}$$

The momentum conservation equation (Navier-Stokes equation) is

$$\frac{\partial}{\partial x_j}(\rho \boldsymbol{u}_i \boldsymbol{u}_j) = -\frac{\partial p}{\partial x_i} + \frac{\partial}{\partial x_j}\left[\mu \frac{\partial \boldsymbol{u}_i}{\partial x_j} - \boldsymbol{\tau}_{ij}\right] + S_i . \tag{2}$$

The energy equation is

$$\frac{\partial}{\partial x_j}(\rho \boldsymbol{u}_j T) = \frac{\partial}{\partial x_j}\left[\frac{K}{c}\frac{\partial T}{\partial x_j}\right] + S_T , \tag{3}$$

where ρ is the gas density, $\boldsymbol{u}_i$ and $\boldsymbol{u}_j$ are the velocity components in the x_i and x_j directions, μ is the dynamic viscosity, $\boldsymbol{\tau}_{ij}$ is Reynolds stress tensor, S_i is the general source term of momentum conservation equation, S_T is the viscous dissipation function, T is the temperature, and K is the thermal conductivity.

According to standard k-ε model, the turbulence kinetic energy k and turbulence kinetic energy dissipation rate ε equations are given as follows:

$$\frac{\partial}{\partial x_i}(\rho \boldsymbol{u}_i k) = \frac{\partial}{\partial x_j}\left[\left(\mu + \frac{\mu_t}{\sigma_k}\right)\frac{\partial k}{\partial x_j}\right] + G_k + G_b - \rho\varepsilon - Y_M + S_k , \tag{4}$$

$$\frac{\partial}{\partial x_i}(\rho \boldsymbol{u}_i \varepsilon) = \frac{\partial}{\partial x_j}\left[\left(\mu + \frac{\mu_t}{\sigma_k}\right)\frac{\partial \varepsilon}{\partial x_j}\right] + C_{1\varepsilon}\frac{\varepsilon}{k} \cdot (G_k + C_{3\varepsilon}G_b) - C_{2\varepsilon}\rho\frac{\varepsilon^2}{k} + S_\varepsilon , \tag{5}$$

where G_k is the generation of turbulence kinetic energy k due to the mean velocity gradients, G_b is the generation of turbulence kinetic energy k due to the buoyance, Y_M is the generation of pulsation expansion in the com-

pressible turbulent flow, μ_t is the turbulence viscosity, and S_k and S_ε are the source terms. The empirical constants in above equations are given as $C_{1\varepsilon} = 1.44$, $C_{2\varepsilon} = 1.92$, $C_\mu = 0.09$, $\sigma_k = 1.0$ and $\sigma_\varepsilon = 1.3$.

3.2 Grid generation

The computation domain grid was created using preprocessing software Gambit. In the actual experimental set-up, the nozzle, the atomization chamber and the enclosed gas flow can be treated as rotational symmetry. Therefore, only half of the flow field was solved, as shown in Figure 2. Rotated by 90° ccw (counter clockwise) from its normal operational orientation, the gas flow field was oriented horizontally. The gas inlet plane was on the left, the outlet plane was on the right, and the axis of symmetry boundary was on the bottom of the computational domain. The grid was generated using quadrilateral elements, which was finer near the nozzle outlet zone as a result of high pressure gradient, and coarse grid was applied to the atomization chamber outlet zone. The contour of nozzle jet was of approximate treatment in stead of complex Laval design. As can be seen in Figure 2, h is the protrusion length of metal delivery tube, h=1 mm, and the jet included angle α is equal to the apex angle β of metal delivery tube, $\alpha = \beta = 90°$.

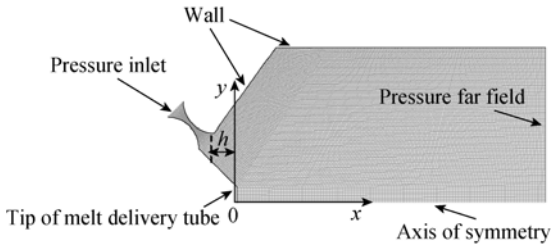

Figure 2 The computational domain of CCSN and boundary conditions.

3.3 Boundary conditions

The boundaries are shown in Figure 2. The nozzle inlet was set as pressure inlet condition, the atomization chamber outlet was set as pressure far field, the centerline of the gas flow field was set as axis of symmetry, and other boundaries including the tip of melt delivery tube were set as walls. The atomization gas pressures P_0 of 15, 20, 25, 30, 35, 40, 45 and 50 atm (1 atm = 1.01×10^5 Pa) at the nozzle inlet were used, and the temperature of gas was 300 K. The atmospheric pressure were used as the outlet pressure P_e, and temperature of gas was 300 K. The pressure P_a in the atomization chamber was the atmospheric pressure. The vertical velocity on the center line of gas field was equal to zero. The gas at all the wall boundaries was assumed to be near-wall flow model, which was dealt with standard wall function. The atomization gas chosen for the study was nitrogen and gas constants were given in Table 1. The gas viscosity was computed using Sutherland viscosity law,

$$\mu = \mu_0 \left(\frac{T}{T_0}\right)^{3/2} \frac{T_0 + S}{T + S}, \tag{6}$$

where μ is viscosity, μ_0 is the reference viscosity, T_0 is the reference temperature, T is the static temperature, and S is the effective temperature, or Sutherland constant. The others were set as the default settings of Fluent.

Table 1 Nitrogen properties for numerical simulation

Physical property	Value
Density (kg/m^3)	1.138
C (J/(kg·K))	1040.67
Thermal conductivity (W/(m·K))	0.0242
Reference viscosity (kg/(m·s))	1.663×10^{-5}
Reference temperature (K)	273.11
Effective temperature (K)	106.67
Molecular weight (kg/(kg·mol))	28.0134
Standard state entropy (J/(kg·mol·K))	191494.8

3.4 Solution method

In this paper the governing equations were discretized using an implicit, second-order upwind scheme and coupling algorithm. In the calculation, a Courant number of 2.0 was selected. The gas flow field simulation required approximately 60000 iterations, and the nozzle inlet pressure was the initial value. When the important variable in the gas field did not change any more, the solution was end.

4 Results and discussion

Figures 3(a)—(c) show the effects of different atomization gas pressures on the velocity contour plots of the gas flow field and Figure 3(d) is the experimental Schlieren photograph of the gas-only flow from an annular nozzle by Espina et al[14]. At an atomization pressure of 15 atm (P_0=15 atm), as soon as the atomization gas leaves the exit path of the nozzle jet, a high velocity gas flow is formed. The gas flow rapidly decelerates to a subsonic state after it experiences a series of shocks.

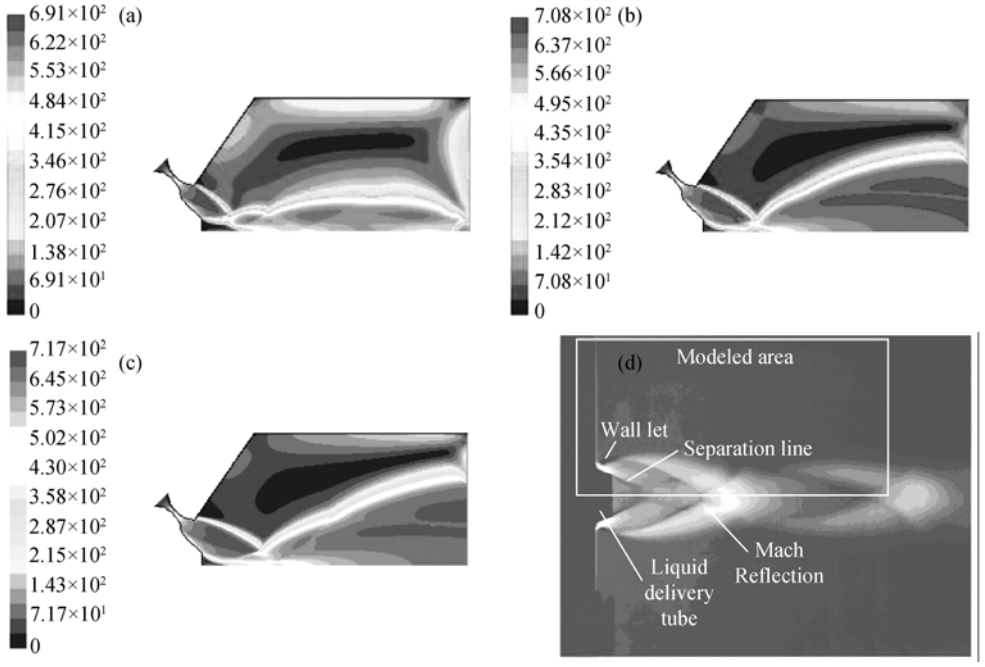

Figure 3 Velocity contour plots at different atomization gas pressures. (a) 15 atm; (b) 20 atm; (c) 25 atm; (d) Schlieren photograph of the gas-only flow from an annular nozzle (reproduced from ref. [14]).

The gas flow field within the sonic boundary (the effective atomization zone) is narrow and Mach disk located at the center line of the gas flow field is obscure or absent, as shown in Figure 3(a). As the atomization gas pressure increases to 20 atm (P_0=20 atm), the gas flow expands through a series of expansion waves and accelerates continually, which makes a wide effective atomization zone appear and a Mach disk form in the centerline, as shown in Figure 3(b). As P_0 up to 25 atm, it can be observed from Figure 3(c) that a diminutive subsonic zone is located at downstream Mach disk, and a wider effective atomization zone is generated. Compared to the experimental Schlieren photograph[14], it is found that agreement between the characteristics of the numerical result and experimental measurement is quite good. The flow field structure for P_0>25 atm is not discussed due to it is similar to that of P_0=25 atm. In addition, it is obvious from Figure 3 that with increasing atomization gas pressure P_0 from 15 to 25 atm, the maximum gas flow velocity increases from 6.91×10^2 m/s to 7.17×10^2 m/s. An explanation for this result is that each nozzle has a design state (or perfect state), namely, the gas flow pressure at the nozzle exit equals the ambient surrounding pressure, and the nozzle is called correctly expanded. However, if the gas flow pressure expanded at the exit is below the ambient surrounding pressure, as shown in Figure 3(a), a shock wave would be formed outside of the nozzle and the gas flow velocity descends in order to match the higher surrounding pressure, and this case is called overexpansion. If the gas flow pressure at the exit is higher than the ambient surrounding pressure, the expanded wave forms at the exit of nozzle, therefore the gas flow is capable of further expanding and accelerating after leaving the nozzle (Figures 3(b) and (c)). Such a case is called underexpansion. It also can be seen in Figure 3 that when the atomization gas pressure P_0 is larger than 20 atm, the area of subsonic zone located at the downstream Mach disk decreases as P_0 increases.

The static pressure curves along the central line of the flow field are presented in Figure 4. It can be seen that as the distance from the tip of melt delivery tube increases, the static pressure decreases until a minimum value is obtained. Then the static pressure rapidly rises to the first maximum pressure (located at stagnation point, named stagnation pressure). After that, it gradually falls for a distance and rises abruptly to a second peak value as the atomization gas crosses Mach disk. The change of static pressure is associated with the structure of gas flow field. The axisymmetric high velocity gas flow converges at the stagnation point located at the central line of the flow field (At this point, the gas

velocity becomes zero and the gas pressure is the highest), and a recirculation zone is formed between the stagnation point and the tip of the melt delivery tube. The velocity vector of the recirculation zone is shown in Figure 5. It is observed that a portion of atomization gas enter the recirculation zone through the stagnation point and the other moves downward away from the tip of the melt delivery tube. The gas flow in the recirculation zone moves toward to the tip of the melt delivery tube due to the existence of a large positive pressure gradient. The gas flow is first accelerated to the maximum and then decelerates because of a negative pressure gradient. When it approaches the tip of the melt delivery tube, the gas flow turns outward radially along the tip of the melt delivery tube and contacts with the sonic gas flow boundary at the rim, which pushes the gas flow inward and moves downstream[8,9]. In this case, some gas flow moves down at the interior of sonic boundary and other moves together with the high velocity atomization gas flow at the exterior of sonic boundary as a result of viscous force. Within the recirculation zone, a turbulent layer separates the upstream and downstream gas flows.

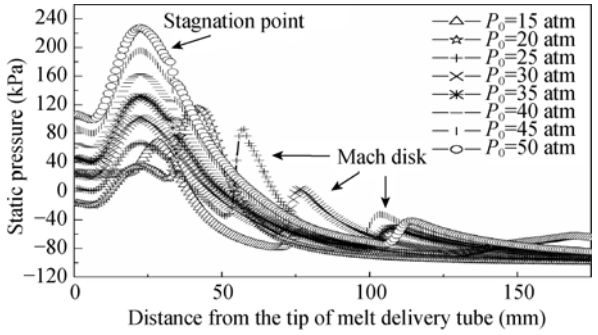

Figure 4 Static pressure curves along the central line of the flow field.

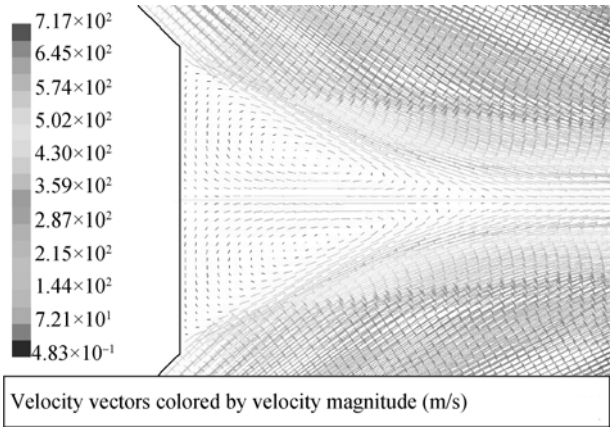

Figure 5 Velocity vectors of the recirculation zone.

Figure 6 is the locations of stagnation point and Mach disk as well as stagnation point pressure in terms of the atomization gas pressure. It can be seen that with increasing atomization gas pressure the positions of stagnation point and Mach disk move towards the tip of the melt delivery tube firstly. This means that the distance from the tip of melt delivery tube to them decreases. However, further increasing the atomization gas pressure the location of Mach disk moves downstream from the tip of the melt delivery tube, and a plateau appears at P_0=35－45 atm. The location of stagnation point does not change essentially as P_0 is above 20 atm. However, the stagnation point pressure decreases with increasing the atomization gas pressure P_0, similar to the change of the position of Mach disk. The result shows that when P_0 is below 20 atm, the cross point of high velocity gas flow and Mach disk moves towards the melt delivery tube. At the same time, the stagnation point pressure at the central line decreases gradually. When P_0 is above 20 atm, Mach disk moves downstream, causing a longer distance from the melt delivery tube. Meanwhile, the cross point of high velocity gas flow does not vary, and the pressure of cross point increases linearly.

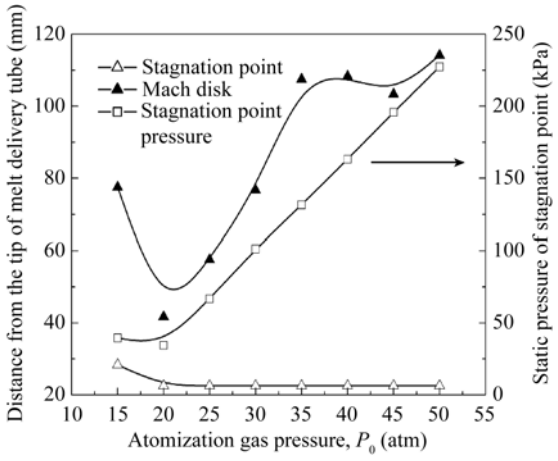

Figure 6 Locations of stagnation point and Mach disk, and stagnation point pressure in terms of atomization gas pressure.

During the atomization process, the relation between the velocity v of the melt flowing out of the crucible and aspiration pressure ΔP can be determined by the following expression,

$$v = \sqrt{2gH - \frac{2\Delta P}{\rho}}, \tag{7}$$

where g is the gravitational constant, 9.81 m/s^2, ρ is the

density of the melt, and H is the height of the metallostatic head. It is obvious from the above equation that if the melt in the crucible is maintained at a constant height of melt head, the velocity v is a function of ΔP during the atomization process. When $\Delta P>0$, the melt flow velocity should be reduced, and in some case the gas would eject melt from the crucible and/or freeze off the melt flow. When $\Delta P<0$, the melt should be sucked into atomization region and the velocity v increases. Figure 7 is the result of ΔP of numerical simulation and experiment with the variety of atomization gas pressure P_0, where $\Delta P=P_t-P_a$, P_t is the pressure at the tip of the melt delivery tube and P_a=1 atm is the atmospheric pressure. The method of experiment was that the pressure transducers A and B were located at the melt delivery tube and the inlet of manifold, respectively, in order to measure the aspiration pressure ΔP at the tip of the melt delivery tube and the atomization gas pressure P_0. The pressure ranges of pressure transducers A and B were −100－600 kPa and 0－10 MPa, respectively. The accuracy of both pressure transducers was ±0.5% of the full scale. During the measurements the pressure port of pressure transducer A was placed inside the metal delivery tube, and then joined to a digital converter, which in turn connected with a computer. From Figure 7 it can be seen that the same trend is observed in the numerical and experimental results: ΔP at first decreases and then increases as the P_0 increases. The result means that the effect of atomization gas pressure can not lead to a progressive decrease in aspiration pressure, thereby strengthing the sucking action. Associated with Figure 6, it is shown that the curve of aspiration pressure is in agreement with those of stagnation point pressure and Mach disk location, but in disagreement with that of the stagnation point location. In the recirculation zone, the aspiration pressure is affected by the mass balance of the gas entering and leaving the recirculation zone[7]. The stagnation pressure is a measure of the amount of gas entering the recirculation zone. Considering the fact that the high stagnation pressure indicates the large density of gas, high stagnation pressure will let more gas enter the recirculation zone, i.e., a high aspiration pressure (the weaken sucting action) can occure. In addition, the recirculation zone is seperated into two parts as a result of the appearance of Mach disk (Figure 3(b)), which blocks the movement of gas flow towards the melt delivery tube[15]. Therefore, the aspiration pressure can be reduced. At high atomization gas pressure (P_0>20 atm), with increasing the atomization gas pressure, the location of Mach disk moves away from the recirculation zone (But the location of stagnation point does not change), so the influence of Mach disk on the pressure of the recirculation zone gradually decreases. It could be assumed that the aspiration pressure coud be directly affected by the stagnation pressure.

However, there are discrepances between numerical and experimental results at the aspiration pressure values and critical atomization gas pressure values, as shown in Figure 7. This phenomenon can be explained as follows. First of all, the accuracy of solution is determined by the number of the cells adopted in the grid; secondly, standard k-ε model used in the flow near the curved wall, such as the contour of gas jet shown in Figure 2, will lead to some skewness; finally, there are differences between the actual atomization nozzle and the numerical model configurations and these will give rise to the change of structure of gas flow field.

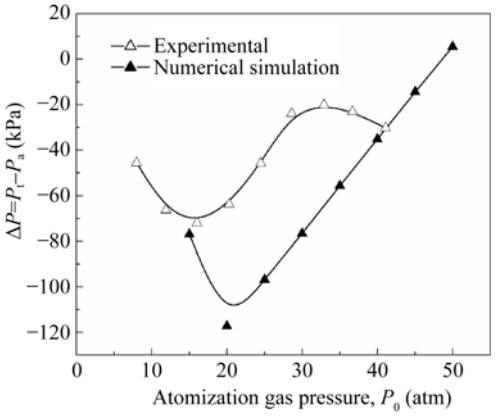

Figure 7 Aspiration pressures ΔP in terms of atomization gas pressures obtained from numerical simulation and experiment.

Figure 8 presents the gas velocity curve along the central line of the flow field. It can be seen that within the recirculation zone, the gas flow velocity at the stagnation point is equal to zero. At the atomization pressure P_0>15 atm, the trend of the variation of gas flow velocity is generally uniform. At P_0=15 atm, the variation of gas flow velocity and the minimum value of gas flow velocity within the recirculation zone are different from those at P_0>15 atm. The gas flow in the recirculation zone moves toward the tip of the melt delivery tube and gradually accelerates due to a large positive pressure gradient exists (A negative velocity indicates that the gas flows in the opposite direction of x axis). After

reaching a maximum value (minimum in the curve), the gas flow decelerates until it is equal to zero when the gas approaches the tip of the melt delivery tube. After the stagnation point (the gas flows in the direction of x axis), the gas accelerates gradually (here positive velocity). The gas flow velocity drops abruptly at the location of Mach disk, then accelerates again after passing through Mach disk. Figure 8 also shows that at atomization gas pressure ΔP=15 atm the gas flow velocity rapidly attenuates at a distance farther than the location of Mach disk and reaches 509.7 m/s at the exit of the gas flow field. However, at P_0>15 atm, the gas flow velocity always accelerates at the downstream Mach disk, and reaches 626.5－672.2 m/s. It must be pointed out that the difference of gas flow velocity at the exit of gas field for different atomization gas pressures is produced by different accelerating distance, which is a result of the location of Mach disk. So it can explain why the gas flow velocity at the exit of the gas flow field decreases as the atomization gas pressure increases. For instance, at P_0=20 atm and 50 atm, the maximum gas flow velocities are 672.2 and 626.5 m/s, respectively.

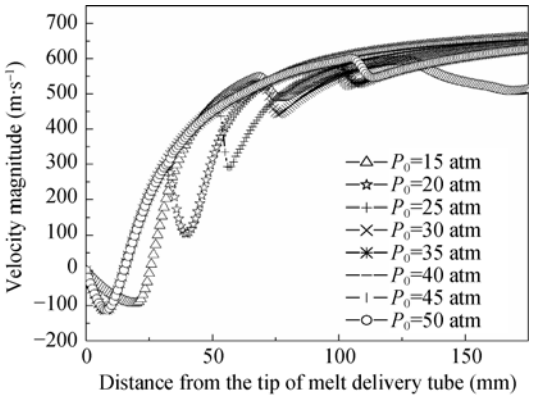

Figure 8 Gas velocity curves along the central axis of the flow field.

Figure 9 illustrates static pressure curves along the tip of the melt delivery tube radically. As shown in the figure, a radical static pressure gradient is presented along the tip of the melt delivery tube and this gradient increases as the atomization gas pressure increases except for P_0=15 atm. The pressure gradient provides evidence for the prefiming mechanism, which is the most commonly quoted and accepted melt break up mechanism[6−8,16]. During the gas atomization process, the radial pressure gradient gives rise to the melt flow to spread and a thin melt film is formed at the edge of the tip of the melt delivery tube. Subsequently, the melt experiences the primary break up as it interacts with the high velocity gas flow. During the primary break up of the melt, large ligaments and sheets are formed, which are subsequently spheroidized caused by the surface tension of the melt and eventually become large melt drops. Previous research works have shown evidence that the size of melt drop depends to a large extent on the thickness of the liquid film at the tip of the delivery tube, atomization gas velocity, etc[6]. At the same gas flow velocity, the thicker the melt film, the greater the size of melt drop produced by primary break up. However, the thickness of melt film is inversely proportional to the radical pressure gradient at the tip of the melt delivery tube, namely a lager pressure gradient gives rise to a smaller thickness of melt film. Accordingly, large pressure gradient may lead to small sized melt drop formed after primary break up. Besides, from Figure 9 it can be seen that with increasing the atomization gas pressure, the aspiration pressure increases to produce a weak sucking action on the melt flow or lead to a low velocity of the melt flowing out of the crucible. A low velocity of the melt gives rise to small thickness of the melt film. Based on the above analysis, it can be found that the high atomization gas pressure leads melt drop size to refine (high atomization efficiency), and the reason lies in the following three aspects: as the atomization gas pressure increases, the gas flow velocity and the dimensionless Weber number determine whether the melt drop experiences breaking up or not, increase; with increasing the aspiration pressure, the flow rate of melt, leading to a large GMR (gas-to-metal ratio); a high pressure gradient at the tip of the melt delivery tube gives rise to a small thickness of melt film.

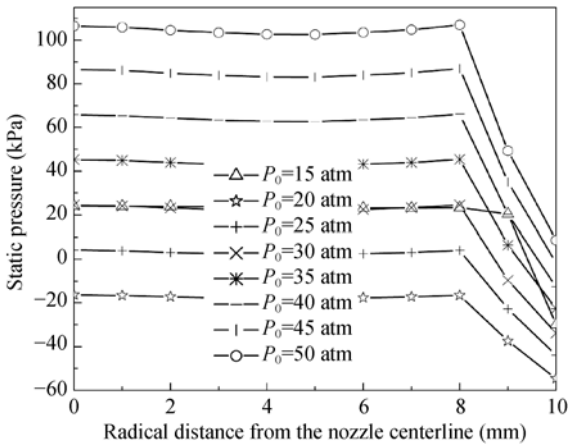

Figure 9 Static pressure curves along the tip of the melt delivery tube radically.

5 Conclusions

1) A numerical model has been developed to simulate the atomization process of close-coupled supersonic atomization nozzle using software Fluent. The results show that the atomization gas pressure has an important influence on the gas flow field. The numerical gas flow field is in good qualitative agreement with experimental Schlieren photograph, indicating that the result can be used to develop the rule and guidance for the design of high efficient atomization nozzle, the operation of atomization nozzle, and the understanding of the phenomena during atomization process.

2) The aspiration pressure decreases and then increases as the atomization gas pressure increases. At P_0>20 atm, with increasing the atomization gas pressure the location of Mach disk moves away from the recirculation zone, so it could be assumed that the aspiration pressure coud be directly affected by the stagnation pressure.

3) A radical static pressure gradient is presented along the tip of the melt delivery tube and this gradient increases as the atomization gas pressure increases.

1 Ouyang H W, Chen X, Yu W T, et al. Progress and prospect on the gas atomization (in Chinese). Powder Metal Technol, 2007, 25(1): 53－63

2 Yu X L, Zhao M Q, Zhao G Y. Influence of atomizing gas pressure on 63A solder powder in supersonic atomization. Powder Metall, 2004, 47(2): 200－204

3 Aksoy A, Ünal R. Effects of gas pressure and protrusion length of melt delivery tube on powder size and powder morphology of nitrogen gas atomized tin powders. Powder Metall, 2006, 49(4): 349－354

4 Singh D D, Dangwal S. Effects of process parameters on surface morphology of metal powders produced by free fall gas atomization. J Mater Sci, 2006, 41(12): 3853－3860

5 Anderson I E, Terpstra R L. Progress toward gas atomization processing with increased uniformity and control. Mater Sci Eng A, 2002, 326(1): 101－109

6 Srivastava V C, Ojha S N. Effect of aspiration and gas-melt configuration in close coupled nozzle on powder productivity. Powder Metall, 2006, 49(3): 213－218

7 Ting J, Peretti M W, Eisen W B. The effect of wake-closure phenomenon on gas atomization performance. Mater Sci Eng A, 2002, 326(1): 110－121

8 Mi J, Figliola R S, Anderson I E. A numerical simulation of gas flow field effects on high pressure gas atomization due to operating pressure variation. Mater Sci Eng A, 1996, 208(1): 20－29

9 Mi J, Figliola R S, Anderson I E. A numerical investigation of gas flow effects on high-pressure gas atomization due to melt tip geometry variation. Metall Mater Trans B, 1997, 28(5): 935－941

10 Jeyakumar M, Gupta G S, Kumar S. Modeling of gas flow inside and outside the nozzle used in spray deposition. J Mater Process Tech, 2008, 203(1-3): 471－479

11 Tong M, Browne D J. Direct numerical simulation of melt-gas hydrodynamic interactions during the early stage of atomization of liquid intermetallic. J Mater Process Tech, 2008, 202(1-3): 419－427

12 Zeoli N, Gu S. Computational simulation of metal droplet break-up, cooling and solidification during gas atomisation. Comp Mater Sci, 2008, 43(2): 268－278

13 Allimant A, Planche M P, Dembinski L, et al. Progress in gas atomization of liquid metals by means of a de Laval nozzle. Powder Technol, 2009, 190(1-2): 79－83

14 Espina P I, Piomelli U. Study of the Gas Jet in a Close-coupled Gas-metal Atomizer. Technical Report, American Institute of Aeronautics and Astronautics, 98-0959. 1998. 1－12

15 Ting J, Anderson I E. A computational fluid dynamics (CFD) investigation of the wake closure phenomenon. Mater Sci Eng A, 2004, 379(1-2): 264－276

16 Ouyang H W, Huang B Y, Chen X, et al. Melt metal sheet breaking mechanism of close-coupled gas atomization. T Nonferrous Met Soc China, 2005, 15(5): 985－992